IEEE Photonics Journal
An IEEE Photonics Society Publication

Open Access

Design of Silicon Photonic Structures for Multi-Site, Multi-Spectral Optogenetics in the Deep Brain

Volume 12, Number 6, December 2020

Roya Nazempour
Qianyi Zhang
Changbo Liu
Xing Sheng

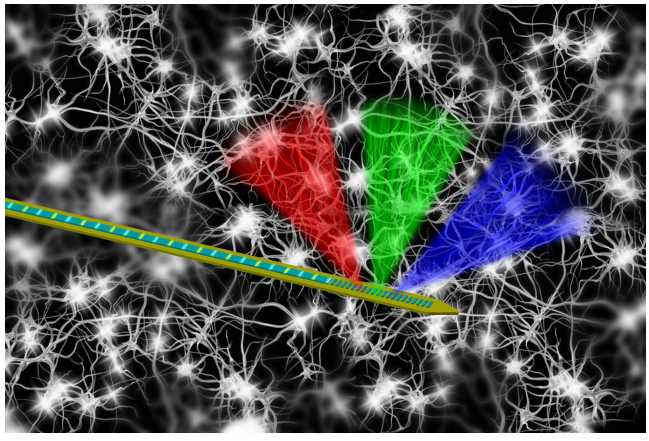

DOI: 10.1109/JPHOT.2020.3039015

IEEE photonics SOCIETY

IEEE

Design of Silicon Photonic Structures for Multi-Site, Multi-Spectral Optogenetics in the Deep Brain

Roya Nazempour,[1] Qianyi Zhang,[1] Changbo Liu,[2] and Xing Sheng [1]

[1]Department of Electronic Engineering, Beijing National Research Center for Information Science and Technology, Center for Flexible Electronics Technology, Tsinghua University, Beijing 100084, China
[2]School of Materials Science and Engineering and Hangzhou Innovation Institute, Beihang University, Beijing 100191, China

DOI:10.1109/JPHOT.2020.3039015

Manuscript received November 5, 2020; accepted November 15, 2020. Date of publication November 18, 2020; date of current version December 9, 2020. This work was supported in part by the National Natural Science Foundation of China under Grant 61874064, in part by Beijing Municipal Natural Science Foundation under Grant 4202032, and in part by Beijing Innovation Center for Future Chips. *(R. Nazempour and Q. Zhang contributed equally to this work.)* Corresponding author: Xing Sheng (e-mail: xingsheng@tsinghua.edu.cn).

Abstract: Micro- and nanoscale photonic structures and devices play important roles in the development of advanced biophotonic systems, in particular, implantable light sources for optogenetic stimulations. In this paper, we numerically investigate silicon (Si) photonics based microprobes that can achieve multi-site, multi-spectral optical excitation in the deep animal brain. On Si substrates, silicon nitride (Si_3N_4) based planar waveguides can deliver visible light in the deep tissue with low losses, and couple to grating emitters diffracting light in targeted brain regions. In our model, we combine near-field wave optic and far-field ray tracing simulations, showing that the designed photonic structures spectrally split blue, green and red photons into different locations in the tissue. Furthermore, by introducing dual grating components, photons at different wavelengths can be spatially separated at different depths. Therefore, these photonic probes can be used to selectively activate or inhibit specific neurons and nuclei, when expressing various corresponding light sensitive opsins. We anticipate that such device strategies can find wide applications in the design of advanced implantable photonic systems for neuroscience and neuroengineering.

Index Terms: Implantable device, silicon photonics, optogenetics.

1. Introduction

Optogenetics plays an indispensable role in the field of neuroscience and neuroengineering for decoding neural signals and modulating neural activities, which could enrich understandings in brain functions and help discover novel strategies for neurological disease treatments [1], [2]. Such optically based neural interrogation methods employ various light-sensitive microbial opsins that exhibit different excitation spectra and control different ion channels, providing precise control over specific neural activities with light modulations at certain wavelengths [3], [4]. As excitation spectra of most opsins typically lie within the visible range, where light penetration is severely limited by the tissue scattering and absorption, advanced waveguides and optoelectronic devices

have been exploited for effective light delivery into the deep tissue [5], [6]. Most commonly used light-guiding method for optogenetics is based on optical fibers made of silica [7], [8] owing to its low cost, high optical transparency and structural stability in biological environments. However, simple silica fibers cannot provide versatile functions like spatially and spectrally resolved light delivery in the tissue, and the high mechanical stiffness of silica often causes unwanted tissue damages and inflammation. Alternative strategies are also proposed, based on polymer waveguides, which exhibit better biocompatibility and even dissolvability within the body [9]–[11]. Recently developed thin-film, microscale optoelectronic devices that can be directly implanted into the animal brain provide alternative promising solutions to advanced optical neural interfaces. By integrating microscale light-emitting diodes (LEDs), photodetectors, and various electronic and chemical sensors onto flexible substrates, as well as wirelessly operated circuit modules, untethered, multifunctional neural probes can be realized [12]–[15]. Nevertheless, challenges associated with electrical heating and device's long-term stability within the tissue remain daunting for these directly implanted active emitters and sensors [16]. Apart from above solutions, planar waveguides based on silicon (Si) and related materials (silicon oxide SiO_2, silicon nitride Si_3N_4, etc.) offer an emerging method for implantable light sources within the animal body. Taking advantage of mature micro- and nano-fabrication techniques recently developed for silicon photonics in the past decade, sophisticated optical components like waveguides, splitters, resonators and couplers, can be fine-tuned to realize miniaturized, compact structures used as implantable optical sources for various functionalities. Remarkable examples include the developments of Si photonics based waveguides, cavities and switchable grating couplers for sensing biomarkers [17], intracranial pressure and temperature [18], and multi-site optogenetic stimulations [19], [20].

With further explorations of the complex neural activities associated to different cell types and brain regions [21], multi-site, multi-spectral light-guiding techniques become crucial in optogenetic studies. By expressing different types of opsins in specific neural cells and brain regions, and employing stimulations by photons with corresponding wavelengths, simultaneous, bi-directional modulations of neural activities for different cells and brain regions are becoming possible. To realize this vision, the design of light emitters for multi-site and multi-spectral stimulation is highly demanded. Recent works have achieved such multi-site stimulation functionalities using multipoint emitting optical fibers [22], fiber bundles [23], micro-LEDs [24] or nanophotonic waveguides [19], [25], and yet only few research focuses on light-guiding systems combining both multi-site and multi-spectral stimulation [26].

In this paper, we propose implantable waveguide structures with grating emitters that can realize multi-site and multi-spectral optical stimulations in the deep brain. Enabled by silicon photonics technology, Si_3N_4 based thin-film waveguides with low losses and diffractive gratings with high coupling efficiencies can be numerically designed and applied to spectrally split emitted photons into different locations when implanted into the brain tissue. Modeling results reveal that outcoupled light with different colors (blue, green and red) can be directed at different emissive angles, and distributed into different tissue locations in the far field accordingly. Furthermore, we also propose a photonic structure that is able to spatially separate blue and red photons and deliver them into different regions via the waveguide. The designed structures provide guidelines for advanced optical neural interfaces, and offer new opportunities to optogenetic interrogations of complex brain functions.

2. Results and Discussions

Fig. 1 illustrates the conceivable design of the implantable photonic probe that can deliver photons of different wavelengths into the animal brain. Based on a silicon substrate, the designed Si_3N_4 waveguide provides high transparency in the visible spectral range, with a grating emitter that diffracts photons at different wavelengths at various angles into the brain tissue.

Fig. 2(a) displays the schematic structures of the waveguide and the grating coupler on the probe tip. The Si_3N_4 waveguide has a width of 20 μm and a thickness of 0.2 μm, embedded in SiO_2. The thicknesses of the top and the bottom SiO_2 layers are 0.66 μm and 5 μm, respectively. The grating

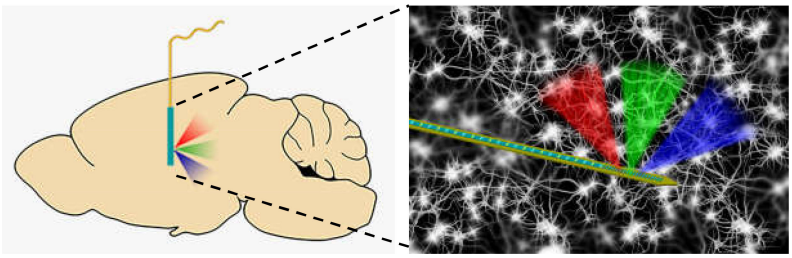

Fig. 1. Conceptual sketch of an implanted waveguide with grating based emitters for multi-site, multi-color optogenetic stimulations in the mouse brain.

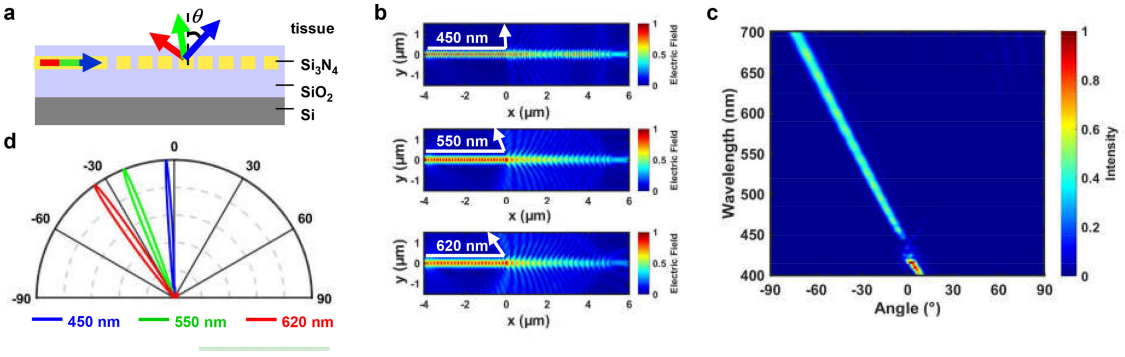

Fig. 2. Optical simulations of light outcoupling for the designed grating emitter, based on the finite-difference time-domain (FDTD) method. (a) Schematic illustration of the waveguide and grating structures, showing that the outcoupled light is spectral split towards different emissive angles. (b) Normalized, near-field electric field distributions around the grating emitter at wavelengths of 450 nm (top), 550 nm (middle) and 620 nm (bottom), respectively. Arrows indicate the propagation directions of the diffracted beams. (c) Far-field emission intensities at various wavelengths and emissive angles. (d) Far-field, angular dependent emission profiles for 3 different wavelengths: 450 nm (blue), 550 nm (green) and 620 nm (red).

emitter has a period $\Lambda = 0.26$ μm, with a 50:50 duty cycle (fill factor $F = 0.5$) and 20 periods. The entire structure is based on a silicon substrate with a thickness less than 50 μm, and can be formed using standard microfabrication processes, including chemical vapor deposition, reactive ion etching, photolithography, wafer thinning, etc. Finite-difference time-domain (FDTD) simulations [27] are utilized to analyze the wave propagation and beam diffraction properties. Optical properties of Si, SiO_2 and Si_3N_4 are quoted from literatures [28], [29]. SiO_2 and Si_3N_4 have refractive indices $n_{\mathrm{SiO2}} = 1.46{\sim}1.47$ and $n_{\mathrm{Si3N4}} = 2.04{\sim}2.08$, respectively, and both are transparent across the visible spectrum. The surrounding environment is assumed to be a biological tissue with a refractive index of 1.36. Since the grating width is much larger than the grating period, a two-dimensional FDTD model is applied to reduce the running time. A source of plane wave from 400 nm to 700 nm in transverse magnetic (TM) mode is coupled to the waveguide. The waveguide loss is calculated to be less than 1 dB/cm. When the wave reaches the grating, light beams are scattered into the tissue, with the first-order diffractive angle θ. Fig. 2(b) presents the profiles of electric field within such a photonic structure at specific wavelengths $\lambda = 450$ nm, 550 nm and 620 nm. Arrows in the graphs indicate the diffractive directions upward into the tissue. The first-order diffractive angle θ can also be calculated analytically

$$n_{\mathrm{SiO2}} \cdot \sin\theta = n_{\mathrm{eff}} - \frac{\lambda}{\Lambda} \tag{1}$$

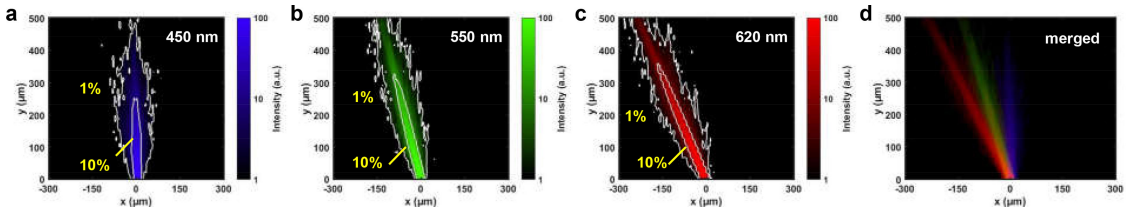

Fig. 3. Optical simulations of light emission from the designed grating emitter to the brain tissue, based on the FDTD results in Fig. 2(d) and the ray tracing method, at various wavelengths: (a) 450 nm; (b) 550 nm; (c) 620 nm, and (d) merged results for the 3 wavelengths, illustrating the spectral splitting effects in the tissue. Iso-intensity lines show 10% and 1% of the maximum power.

where the effective index of the grating n_{eff} is defined as

$$n_{\text{eff}} = F \cdot n_{\text{Si3N4}} + (1 - F) \cdot n_{\text{SiO2}} \tag{2}$$

For blue (450 nm), green (550 nm) and red (620 nm) photons, diffractive angles of this grating are determined to be $-3.4°$, $-21.4°$ and $-35.3°$, respectively. The corresponding diffraction efficiencies are extracted from the FDTD models, which are 26.3%, 40.7% and 43.5%. It should be noted that almost half of the diffractive waves go downwards and absorbed by the Si substrate, and the results can be further optimized, for example, by applying a metal mirror or a Bragg reflector between the Si substrate and the SiO_2 cladding layer. Angular-dependent, far-field diffraction intensity distributions can be further determined, as plotted in Fig. 2(c). Fig. 2(d) presents the results for the three representative wavelengths (450 nm, 550 nm and 620 nm). In agreement with calculations based on Eq. (1), the first-order diffractive angle increases with the wavelength from 450 nm to 700 nm, and diffraction beams are highly collimated ($\pm 1.6°$ for 450 nm, $\pm 2.2°$ for 550 nm, and $\pm 2.6°$ for 620 nm). Such a design presents much smaller divergence compared with conventional light-guiding methods based on implantable fibers ($>10°$) and microscale LEDs ($>120°$); therefore, it allows light beams to be more efficiently focused on targeted nuclei or regions.

To predict the performance of the aforementioned waveguides and grating emitters within the brain tissue, models based on the Monte-Carlo ray tracing method [30] are established, with results presented in Fig. 3. The area of the grating emitter is set to be 20 μm $\times$ 20 μm, within a tissue assumed to be the grey matter of animal brains (refractive index $\sim$1.36). Results at the same three wavelengths (450 nm, 550 nm and 620 nm) as those used in Fig. 2 are modeled. Scattering and absorption coefficients at these wavelengths are (13.13, 8.7 and 7.2 /mm), and (0.38, 0.28, and 0.10 /mm), respectively [28], and the anisotropy of scattering is assumed to be 0.85 (highly forward scattering). Angular-dependent emission profiles are collected from the simulated far-field results shown in Fig. 2(d), of which the emission peaks at diffractive angles of $-3.4°$, $-21.4°$ and $-35.3°$, respectively. A total of 10^5 rays are employed to simulate each wavelength. Figs. 3(a)–3(c) illustrate optical propagations at the three distinct wavelengths, and one can observe the light attenuation associated with the scattering and absorption within the tissue. Penetration depths (at which the optical intensity falls to 1/e $\approx$ 0.368 of the original value) are estimated to be 126 μm, 155 μm and 182 μm, for blue (450 nm), green (550 nm) and red (620 nm) photons, respectively. Fig. 3(d) further depicts optical emissions from the three distinct colors, which clearly reveals that photons at different wavelengths can be split into different parts of the brain tissue. The emission of each colored beam can cover a specifically targeted nucleus, which typically range from tens to hundreds of micrometers in the mammalian brain. By expressing light sensitive opsins (for example, ChR2 for blue, C1V1 for green and Chrimson for red [31]) in specific neurons at different locations, we could realize optical excitation and inhibition of different cell types, thereby modulating neural activities with more freedom compared to previous devices based on monochromatic stimulation.

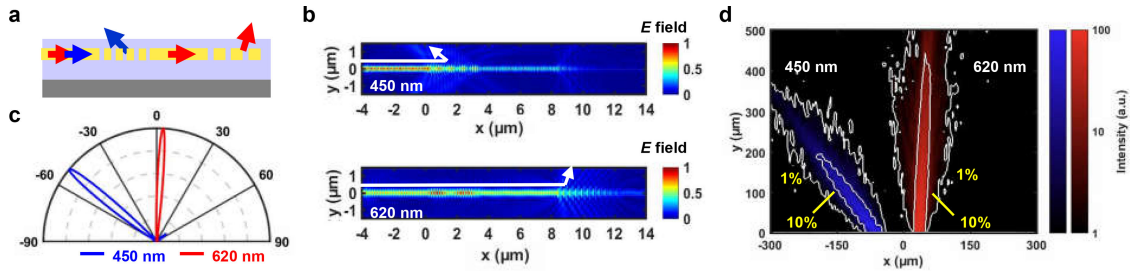

Fig. 4. Design of a grating emitter that delivers blue and red light at different locations. (a) Schematic illustration of the double grating coupler. (b) Normalized, near-field electric field distributions around the grating coupler at wavelengths of 450 nm (top) and 620 nm (bottom), respectively. Arrows indicate the propagation directions of the diffracted beams. (c) Far-field, angular dependent emission profiles for the two wavelengths: 450 nm (blue) and 620 nm (red). (d) Ray tracing results showing spectrally split emissions from the double grating coupler to the brain tissue. The distance between the two gratings is assumed to be around 100 μm. Iso-intensity lines show 10% and 1% of the maximum power.

By leveraging the spectral-dependent diffraction properties of the grating emitter, we can further create a waveguide structure that delivers multispectral photons at different depths into the brain tissue. As shown in Fig. 4(a), the photonic structure consists of two gratings emitting blue (450 nm) and red (620 nm) light, respectively, which are connected by a planar waveguide and based on the same material system as in Fig. 2(a). The first grating (on the left) is designed to have a period of 163 nm (20 periods) and a duty cycle of 60:40 (Si_3N_4:SiO_2). Based on Eq. (1), its first-order diffractive angle for blue photons (450 nm) can be obtained to be $-50.3°$ with beam divergence of 4.0° and its diffraction efficiency is 42.0%, while red photons (620 nm) can transmit through it with minimum scattering. The transmission efficiencies for 405 nm and 620 nm are 16.0% and 95.0%. The second grating (on the right) has a period of 406 nm (10 periods) and a duty cycle of 50:50, which outcouples red photons (620 nm) at a diffractive angle of 3.3° with beam divergence of 2.7° and its diffraction efficiency is 43.9%. Fig. 4(b) shows simulated electric field distributions of such a double grating structure at 450 nm and 620 nm, based on the FDTD method. To reduce the simulation time, the planar waveguide between the two gratings has a length of 4.8 μm. Far-field, angular-dependent emission profiles are plotted in Fig. 4(c). We further evaluate the light emission properties of such a double grating coupler within the brain tissue based on the Monte-Carlo ray tracing method (Fig. 4(d)). Different from the FDTD simulations, the distance between the two gratings is increased to 100 μm. In practice, the grating separation can be tuned based on the locations of targeted brain regions, which will not affect the results, since the waveguide loss is negligible within a few millimeters. The spatially separated photon emissions clearly demonstrate that brain regions at different positions can be targeted, by expressing corresponding opsins in the specific cells and nuclei.

3. Conclusion

To summarize, here we present the numerical design of silicon photonic structures that can form an implantable optical neural interface and realize multi-site, multi-spectral stimulation of neural activities. Moving forward, the fabrication of this nanophotonic device is compatible with the standard complementary metal oxide semiconductor (CMOS) process. The application of such Si based nanophotonic technologies permits the molding of light flow with high spatial-temporal resolutions, low divergence and versatile adjustability for optical neural modulations. Another unique feature of such thin-film Si based implants stems from the biocompatibility and aqueous degradation of Si related materials [17] showing the promise of physical transience in a controlled manner in vivo [32]. Other explorable applications include periscleral crosslinking [33] and phototherapy [34], [35], as demonstrated previously using polymer fibers. Additionally, reconfigurable photonic structures

based on electronically, thermally, and/or mechanically activated devices could be incorporated to obtain tunable emission wavelengths or angles. The system platform also allows the integration with other electronic and photonic components, such as recording electrodes [24], microscale LED and detectors [36], and even microfluidic channels [37] and electrochemical sensors [14]. The results presented here show promising paths to utilize the-state-of-the-art nanophotonic technologies for advanced neural stimulators and medical sensors in general.

References

[1] K. M. Tye and K. Deisseroth, "Optogenetic investigation of neural circuits underlying brain disease in animal models," *Nat. Rev. Neurosci.*, vol. 13, no. 4, pp. 251–266, Apr. 2012.
[2] H. Zhang and A. E. Cohen, "Optogenetic approaches to drug discovery in neuroscience and beyond," *Trends Biotechnol.*, vol. 35, no. 7, pp. 625–639, Jul. 2017.
[3] K. Deisseroth, "Optogenetics: 10 years of microbial opsins in neuroscience," *Nat. Neurosci.*, vol. 18, no. 9, pp. 1213–1225, Sep. 2015.
[4] N. C. Klapoetke *et al.*, "Independent optical excitation of distinct neural populations," *Nat. Methods*, vol. 11, no. 3, pp. 338–346, Mar. 2014.
[5] S. B. Goncalves, J. F. Ribeiro, A. F. Silva, R. M. Costa, and J. H. Correia, "Design and manufacturing challenges of optogenetic neural interfaces: A review," *J. Neural Eng.*, vol. 14, no. 4, Aug. 2017, Art. no. 041001.
[6] H. Xu, L. Yin, C. Liu, X. Sheng, and N. Zhao, "Recent advances in biointegrated optoelectronic devices," *Adv. Mater.*, vol. 30, no. 33, Aug. 2018, Art. no. 1800156.
[7] L. A. Gunaydin *et al.*, "Natural neural projection dynamics underlying social behavior," *Cell*, vol. 157, no. 7, pp. 1535–1551, Jun. 2014.
[8] A. G. Mignani and F. Baldini, "In-vivo biomedical monitoring by fiber-optic systems," *J. Lightw. Technol.*, vol. 13, no. 7, pp. 1396–1406, Jul. 1995.
[9] A. Gierej *et al.*, "On the characterization of novel step-index biocompatible and biodegradable poly(D,L-lactic acid) based optical fiber," *J. Lightw. Technol.*, vol. 38, no. 7, pp. 1905–1914, Apr. 2020.
[10] R. Fu *et al.*, "Implantable and biodegradable Poly(l-lactic acid) fibers for optical neural interfaces," *Adv. Opt. Mater.*, vol. 6, no. 3, Feb. 2018, Art. no. 1700941.
[11] R. Nazempour, Q. Zhang, R. Fu, and X. Sheng, "Biocompatible and implantable optical fibers and waveguides for biomedicine," *Materials*, vol. 11, no. 8, Aug. 2018, Art. no. 1283.
[12] L. Li *et al.*, "Heterogeneous integration of microscale GaN light-emitting diodes and their electrical, optical, and thermal characteristics on flexible substrates," *Adv. Mater. Technol.*, vol. 3, no. 1, Jan. 2018, Art. no. 1700239.
[13] Y. Zhao *et al.*, "Wirelessly operated, implantable optoelectronic probes for optogenetics in freely moving animals," *IEEE Trans. Electron Devices*, vol. 66, no. 1, pp. 785–792, Dec. 2018.
[14] C. Liu *et al.*, "A wireless optoelectrochemical probe for optogenetics stimulation and dopamine detection," *Microsyst. Nanoeng.*, vol. 6, 2020, Art. no. 64.
[15] T. Kim *et al.*, "Injectable, cellular-scale optoelectronics with applications for wireless optogenetics," *Science*, vol. 340, no. 6129, pp. 211–216, Apr. 2013.
[16] P. S. Yarmolenko *et al.*, "Thresholds for thermal damage to normal tissues: An update," *Int. J. Hyperthermia*, vol. 27, no. 4, pp. 320–343, Jun. 2011.
[17] W. Bai *et al.*, "Bioresorbable photonic devices for the spectroscopic characterization of physiological status and neural activity," *Nat. Biomed. Eng.*, vol. 3, no. 8, pp. 644–654, Aug. 2019.
[18] J. Shin *et al.*, "Bioresorbable optical sensor for monitoring of interacranial pressure and temperature," *Sci. Adv.*, vol. 5, no. 7, Jul. 2019, Paper eaaw1899.
[19] A. Mohanty *et al.*, "Reconfigurable nanophotonic silicon probes for sub-millisecond deep-brain optical stimulation," *Nat. Biomed. Eng.*, vol. 4, no. 2, pp. 223–231, Feb. 2020.
[20] B. Li, K. Lee, S. C. Masmanidis, and M. Li, "A nanofabricated optoelectronic probe for manipulating and recording neural dynamics," *J. Neural Eng.*, vol. 15, no. 4, pp. 046008.1–046008.8, May 2018.
[21] G. Buzsáki *et al.*, "Tools for probing local circuits: High-density silicon probes combined with optogenetics," *Neuron*, vol. 86, no. 1, pp. 92–105, Apr. 2015.
[22] F. Pisanello *et al.*, "Multipoint-emitting optical fibers for spatially addressable in vivo optogenetics," *Neuron*, vol. 82, no. 6, pp. 1245–1254, Jun. 2014.
[23] Y. Sych, M. Chernysheva, L. T. Sumanovski, and F. Helmchen, "High-density multi-fiber photometry for studying large-scale brain circuit dynamics," *Nat. Methods*, vol. 16, pp. 553–560, Jun. 2019.
[24] F. Wu, E. Stark, P. C. Ku, K. D. Wise, G. Buzsáki, and E. Yoon, "Monolithically integrated μLEDs on silicon neural probes for high-resolution optogenetic studies in behaving animals," *Neuron*, vol. 88, no. 6, pp. 1136–1148, Dec. 2015.
[25] Y. Son *et al.*, "In vivo optical modulation of neural signals using monolithically integrated two-dimensional neural probe arrays," *Sci. Rep.*, vol. 5, no. 1, Oct. 2015, Art. no. 15466.
[26] K. Kampasi *et al.*, "Dual color optogenetic control of neural populations using low-noise, multishank optoelectrodes," *Microsyst. Nanoeng.*, vol. 4, no. 1, Jun. 2018, Art. no. 10.
[27] A. Taflove and S. C. Hagness, *Computationai Electrodynamics*. Norwood, MA, USA: Artech House, Jun. 2000.
[28] E. S. Gebhart, W. Lin, and A. Mahadevan-Jansen, "In vitro determination of normal and neoplastic human brain tissue optical properties using inverse adding-doubling," *Phys. Med. Biol.*, vol. 51, no. 8, Mar. 2006, Art. no. 2011.
[29] K. Luke, Y. Okawachi, M. R. Lamont, A. L. Gaeta, and M. Lipson, "Broadband mid-infrared frequency comb generation in a Si_3N_4 microresonator," *Opt. Lett.*, vol. 40, no. 21, pp. 4823–4826, Nov. 2015.

[30] S. L. Jacques and L. Wang, *Monte Carlo Modeling of Light Transport in Tissues*. Berlin, Germany: Springer U.S., 1995.
[31] H. Yawo, H. Kandori, and A. Koizumi, *Optogenetics: Light-sensing proteins and Their Applications*. Berlin, Germany: Springer, Jun. 2015.
[32] S. W. Hwang *et al.*, "A physically transient form of silicon electronics," *Science*, vol. 337, no. 6102, pp. 1640–1644, Sep. 2012.
[33] S. J. J. Kwok *et al.*, "Flexible optical waveguides for uniform periscleral cross-linking," *Invest. Ophthalmol. Vis. Sci.*, vol. 58, pp. 2596–2602, 2017.
[34] S. Nizamoglu *et al.*, "Bioabsorbable polymer optical waveguides for deep-tissue photomedicine," *Nat. Commun.*, vol. 7, Jan. 2016, Art. no. 10374.
[35] Y. Jiang *et al.*, "Green light-based photobiomodulation with an implantable and biodegradable fiber for bone regeneration," *Small Methods*, vol. 4, no. 7, Jul. 2020, Art. no. 1900879.
[36] L. Lu *et al.*, "Wireless optoelectronic photometers for monitoring neuronal dynamics in the deep brain," *Proc. Nat. Acad. Sci.*, vol. 115, no. 7, pp. E1374–E1383, Feb. 2018.
[37] J. W. Jeong *et al.*, "Wireless optofluidic systems for programmable in vivo pharmacology and Optogenetics," *Cell*, vol. 162, no. 3, pp. 662–674, 2015.